INSTITUTO SUPERIOR TÉCNICO

UNIVERSIDADE DE LISBOA

1º Semester 2023/2024

Computational Fluid Mechanics

3rd Computational Exercise: Study of Coflow Airfoils in Star CCM+

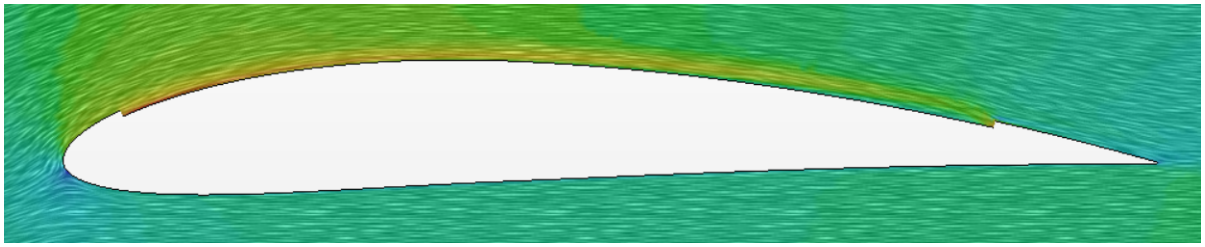

GROUP NUMBER 7

João Fernandes Marques, 93270

Miguel Dias Casalinho, 93307

João Pedro Sousa Gaspar, 96930

Pedro Afonso Simões Gonçalves, 105745

22 December 2023

Contents

1 Introduction

The aerodynamic performance of airfoils, particularly their ability to generate lift and minimize drag, plays a crucial role in the efficiency of the aircraft. However, airfoils can encounter various challenges, including flow separation and dynamic stall, which can significantly reduce their performance. Understanding and managing flow separation is crucial in designing more aerodynamically efficient structures and optimizing fluid flow in various engineering applications that require high lift operations.

1.1 Aerodynamic problem

In fluid dynamics, flow separation is a phenomena in which a fluid, such as air or water, fails to follow the curved contour of a surface and separates, resulting in areas of reversed or recirculating flow. When the fluid comes into contact with adverse pressure gradients, sudden changes in surface curvature, or flow disruptions, this separation usually happens. The thin layer of fluid next to the surface known as the boundary layer may split from the surface if the fluid's kinetic energy is insufficient to overcome these unfavorable conditions. The performance and efficiency of hydrodynamic or aerodynamic systems, such as airfoils, aircraft wings, or undersea surfaces, can be negatively impacted by this separation since it can result in the creation of turbulence, eddies, and vortices which dissipate energy.

To address these issues, Studies have been conducted to investigate flow control techniques for improving the aerodynamic performance of airfoils. Some flow control techniques do not require external energy and instead rely on modifying the airfoil's geometry or surface properties to alter the flow pattern around it.

1.2 Circulation Control and the Co-flow jets

In the pursuit of improving aerodynamic performance, researchers investigating flow control techniques for airfoils have delved into innovative concepts such as circulation control (CC). Circulation control involves blowing while leveraging the Coanda effect. This method manipulates airfoil surface flow, aiming to impart momentum but with energy expenditure and potential thrust penalties. Proposed enhancements include pulsed jets and net-zero-mass-flux synthetic jets as substitutes for continuous jets, though their practical utility is limited. Challenges persist in optimizing these techniques for efficiency in augmenting lift and stall margin.

The co-flow jet airfoil (CFJ) represents a groundbreaking advancement in flow control methods, as discussed in recent studies [1] [2]. In contrast to traditional circulation control (CC) airfoils, which rely on large leading or trailing edges for the Coanda effect, the CFJ technique introduces a novel approach by strategically placing suction and blowing jets along the airfoil's surface. The CFJ induces turbulent shear layers, enhancing lateral energy transport and effectively controlling the boundary layer to delay flow separation.

The key advantage of the CFJ approach lies in its zero net mass flux flow control, minimizing power consumption while outperforming traditional methods such as CC and synthetic jet flow control. The CFJ airfoil efficiently energizes the main flow, overcoming adverse pressure gradients, improving circulation, and achieving lift enhancement, stall margin increase, and drag reduction. Moreover, its versatility allows application to airfoils of varying geometries, promising superior efficiency for higher angles of attack. Recent studies, including NASA's findings on lift improvement [3], underscore the CFJ's potential to significantly enhance aerodynamic performance in diverse applications.

In the realm of flow control, the co-flow jet airfoil (CFJ) stands out as a promising and innovative approach. Unlike conventional methods such as circulation control (CC) airfoils, CFJ strategically employs a combination of suction and blowing jets along the airfoil's surface to control the boundary layer and delay flow separation. This unique configuration, drawing inspiration from the principles discussed in previous research [1] [2], allows CFJ to effectively suppress flow separation over a wide range of angles of attack, including high angles where other techniques may be less effective.

The simplicity of integration into airfoil structures, coupled with its efficiency in terms of energy consumption, makes CFJ a cost-effective and practical solution for various applications, especially in aircraft design. Recent studies, including those conducted by NASA [3], showcase CFJ's potential to significantly improve aerodynamic performance by increasing lift

at high angles of attack and reducing drag at low angles of attack. The CFJ airfoil's ability to enhance performance across different flight conditions positions it as a promising candidate for advancing the efficiency and effectiveness of flow control technologies in aerospace engineering.

The goal of this work is to apply CFJ airfoil technology to a baseline airfoil using numerical simulation with Star CCM+. We will perform different simulations with different angles of attack and mass flow rates to compare the aerodynamic performance of the CFJ airfoil to the baseline airfoil.

2 State Of the Art

The exploration of Co-Flow Jet (CFJ) technology across multiple studies reveals significant advancements in airfoil performance. A comparative analysis of key findings from various papers illuminates the versatile benefits of CFJ across different applications.

One paper introduces the concept of CFJ in high-performance airfoils, emphasizing its superiority in lift enhancement, stall margin improvement, and drag reduction. The study showcases the potential of smaller injection slot sizes to outperform larger ones, underlining the importance of geometry in CFJ airfoil performance [1].

Another study extends the analysis to pitching airfoils through numerical simulations, demonstrating a 32% increase in lift and an 80% decrease in drag with CFJ. The paper explores dynamic stall suppression, emphasizing the feasibility of CFJ helicopter blades. Additionally, it provides insights into the synergistic merits of CFJ technology in comparison to baseline airfoils, with an emphasis on the impact on pressure coefficients, Mach contours, and aerodynamic characteristics [4].

Shifting focus to low-thickness airfoils, a study showcases wind tunnel tests on a modified Clark-Y airfoil. The research highlights CFJ's ability to significantly increase lift (up to 40%) and extend the stall margin, particularly at higher angles of attack. Computational models align with experimental results, reinforcing the potential of CFJ in exploring critical parameters for airfoil design [5].

Another paper introduces a novel subsonic airfoil flow control technique using CFJ, emphasizing its energy efficiency and effectiveness in reducing adverse pressure gradients. The study outlines advantages such as fuel savings, short-distance takeoff and landing, and applicability to low and high-speed aircraft. The comparison with circulation control (CC) airfoils underscores the potential fuel consumption savings of CFJ technology [6].

A comprehensive overview of the impact of CFJ on airfoil performance through control volume analysis and computational fluid dynamics simulations is provided in another study. The research compares CFJ airfoils with injection-only variants, emphasizing the superiority of CFJ in enhancing lift, reducing drag, and improving aerodynamic efficiency. The role of suction on the airfoil surface is identified as a crucial factor in these improvements [2].

Collectively, these studies underscore the broad spectrum of advantages offered by CFJ technology. Smaller injection slot sizes, dynamic stall suppression, lift enhancement in low-thickness airfoils, and subsonic flow control are highlighted. The comparisons reveal a consistent theme of improved lift, reduced drag, and enhanced aerodynamic efficiency across various airfoil designs and applications. The ease of implementation, minimal propulsion system penalty, and applicability to different speed regimes position CFJ as a promising technology for next-generation advanced aircraft design.

3 General Numerical Setup

The computational domain used consists in a bullet shaped domain where the airfoil, with a chord $c = 1m$, was centered with the half circle. Following the optimal setup of [1], the coflow airfoil had a cut depth of 0.6% of c, which ranged from 5% to 85% of c. The selected mesh was triangular, with inflation layers on the airfoil surface. General grid topology as well as mesh local details can be seen in the appendix in Figs. 6-9.

Reynolds number of the simulations was $3x10^6$ to allow validation with experimental data available for the NACA 4412. This leads to a inlet velocity of 45m/s, whose entrance angle was varied in order to simulate the different angles of attack, air density $\rho = 1.225kg/m^3$ and dynamic viscosity $\mu = 1.855x10^{-5}Pa/s$. Inlet condition were defined in both the semicircle and the upper and lower limits of the domain. Outlet was set with gauge pressure equal to zero. For the airfoil, no slip condition

was given to the majority of its surface with the exception of the jet inlet surface, which had a constant profile inlet condition with variable speed considering the configuration used and the suction portion of the airfoil, which has a constant mass flow rate defined to equal the injected one. This mass flow rate is calculated by the expression in equation 1 , where d represents the depth of the airfoil cut and U_{jet} the velocity of the coflow jet at the inlet.

$$\dot{m} = -\rho d U_{jet} \tag{1}$$

Two additional transport equations for turbulence modeling are solved in addition to the standard Reynolds Averaged Navier Stokes equations. This model was the k-w SST which is commonly used in industry for flows in adverse pressure gradients and even in separation conditions, so its used for the present problem seems adequate. Turbulence intensity at the inlet was set as 5% with eddy viscosity ratio of 1. The segregated flow solution method was used since the flow is incompressible.

Simulations were considered converged when residuals were bellow 1e-4 except for more difficult cases where convergence was compromised by big separation of the flow. In this cases residuals bellow 1e-3 were considered sufficiently low to take conclusions on the technology studied. In addition to this, constant behaviour of relevant aerodynamic parameters, such as lift coefficient and drag coefficient was also a requirement to assert sufficient convergence. In cases in which transient behaviour was very prevalent, an implicit unsteady simulation was used instead of the steady-state, with a time step of 1ms and 20 inner iterations in each time step.

4 Grid Convergence Study and Data Validation

In this section, the first steps are taken in order to choose a grid size and topology deemed appropriate for the simulations. This is necessary to be able to "trust" on the results and take meaningful conclusions on the problem. Ideally, this process would have been necessary for every angle of attack and jet flow velocity but due to time constraints, solely one of these configurations was analysed, that is, with a jet velocity of 90m/s and angle of attack of 10 degrees. The group feels confident, however, that the conclusions from this singular refinement study can be extrapolated to the other flow configurations.

4.1 Grid Convergence Study

In order to assess the mesh independence of the results, the mesh was systematically refined until reaching a level where further refinements would not significantly alter the obtained outcomes. For the same airfoil geometry, both for the NACA 4412 case (table 1) and for the airfoil with injection and suction (table 2), three grids for each airfoil with progressively increasing cell counts (A, B, C) were employed for a grid convergence study. The number of cells, denoted as N, for each grid is presented in the tables 1 and 2. The grids underwent refinement by reducing the overall base size of cells and increasing the number of prism layers. For example, for the coarser mesh, less prism layers were used than for the medium and finer ones. These details are also represented in the tables 1 and 2. Nevertheless, the requirements of y^+ were consistently considered to ensure an accurate discretization of the boundary layer flow.

Mesh	**Refinement Level**	**Base Size**	**N**	**Inflation Layers**	C_l
A	**Coarse**	0.01	46085	30	1.4388
B	**Medium**	0.007	99505	42	1.4199
C	**Fine**	0.005	176504	58	1.4079

Table 1: Parameters of the different meshes for NACA 4412 airfoil and their corresponding values of C_l.

Mesh	Refinement Level	Base Size	N	Inflation Layers	C_l
A	**Coarse**	0.008	212668	30	1.6905
B	**Medium**	0.0057	417997	42	1.7199
C	**Fine**	0.004	823660	58	1.7319

Table 2: Parameters of the different meshes for Coflow Jet airfoil and their corresponding values of C_l.

The information in the figure 1 suggest that the computed solutions presented in tables 1 and 2 gradually approach the estimated "true" solution, determined using the Richardson Extrapolation method for both cases. It is crucial to note that a refinement factor of 1.4 was employed, meaning that for instance, in the NACA 4412, the base size of the medium mesh would be $0.01/1.4$, with the base size of the coarse mesh set at 0.01, and so forth.

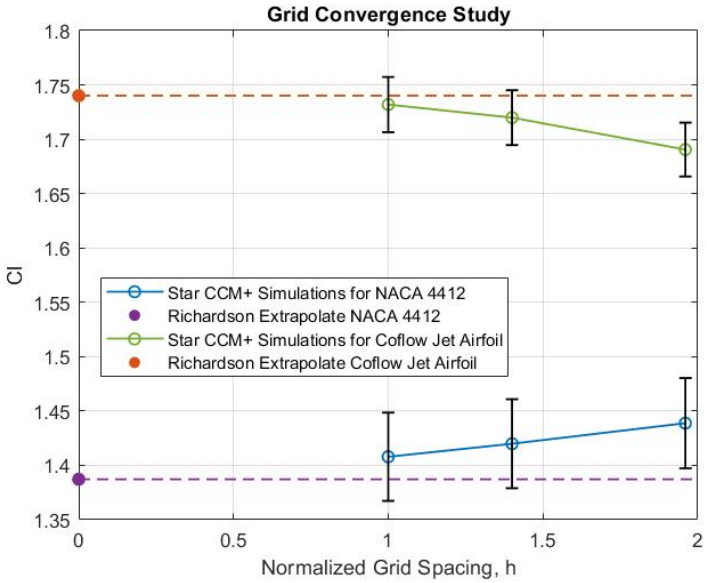

Figure 1: Grid Convergence Study for both cases.

To calculate the Richardson extrapolation, the formula 2 was utilized, considering the C_l values obtained from various simulations conducted in the Star CCM+ software, along with the refinement factor, r.

$$C_{l_{true}} = C_{l_{fine}} + \frac{C_{l_{fine}} - C_{l_{Medium}}}{r^p - 1} \tag{2}$$

For these calculation, the constant p was determined based on the C_l values, as indicated in the formula 3.

$$p = \ln\left(\frac{(C_{l_{Coarse}} - C_{l_{Medium}})}{(C_{l_{Medium}} - C_{l_{Fine}})}\right) / \ln(r) \tag{3}$$

Subsequently, the mesh convergence index (CGI) was computed by the expression 4, both for the refinement from coarse to medium mesh ($GCIA,B$) and from medium to fine mesh ($CGI_{B,C}$) with $F_s = 1.25$ being the safety factor and $|e|$ the error between the meshes, aiming to assess the uncertainty in the computed solution and determine if the simulation exhibits asymptotic behavior, proven by the relation represented in 5.

$$GCI = \frac{F_s|e|}{r^p - 1} \tag{4}$$

$$\frac{GCI_{A,B}}{r^p \times GCI_{B,C}} = 1 \tag{5}$$

These essential parameters required for calculating the true solution and the values obtained for the CGI are presented in the table 3.

	Refinement Factor	p	**Richardson Solution**	$GCI_{A,B}$	$CGI_{B,C}$	**Asymptotic Convergence**
NACA 4412	1.4	1.3566	1.3872	2.88	1.84	0.9915
Coflow Jet	1.4	2.6718	1.7401	1.47	0.59	1.0070

Table 3: Relevant quantities for the calculation of $C_{l_{true}}$ and the study of grid convergence.

Error bars (black lines) shown in figure 1 are computed using Grid Convergence Index (GCI) values. These bars represent the uncertainty in the computed solution and the values $GCI_{A,B}$ were used for both cases, which is already a satisfactory level of uncertainty. A mesh is suitable for use in further simulations, if the true solution falls within the uncertainty range of computed solution from a given mesh. According to figure 1, medium (B) and fine (C) grids are suitable for further computations. Given the availability of limited computational resources, the medium grid (B) was selected as the converged grid for the remainder of this study. Also, by applying the equation to check for asymptotic convergence (equation 5), it yields for both cases ≈ 1. This confirms the solutions are within the asymptotic range of convergence.

4.2 Data Validation

After the verification process described on the previous section, the data obtained by the second grid for the NACA 4412 is validated against experimental data present at the *Summary of Airfoil Data* [7].

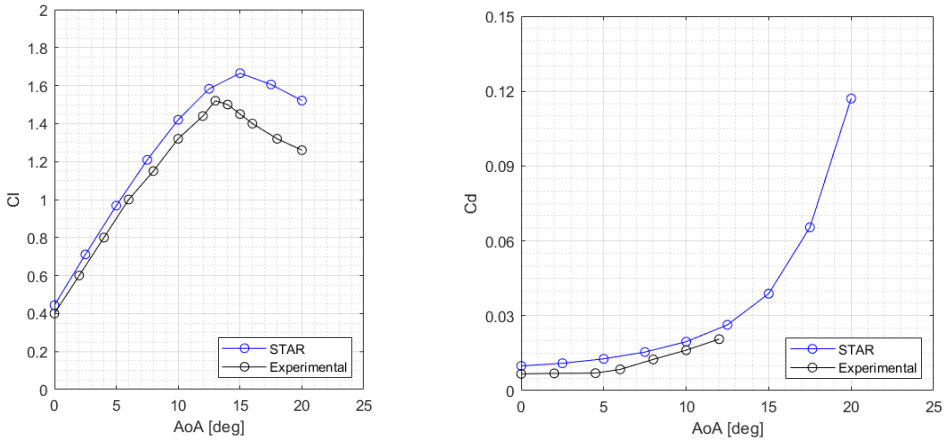

Figure 2: NACA 4412 validation results

As can be seen by the two plots in Figure 2, the numerical results show good accordance with the experimental data available. Lift coefficient is slightly over predicted with the largest relative error being 8% in the region before stall. After the experimental stall angle, Cl deviates significantly more. In the same way, drag coefficient is also above the expected but shows similar behaviour as angle of attack increases.

Due to this, the simulation set ups used were deemed adequate for the rest of this study.

5 Results and Discussion

In this section, the results for the different configurations as well as for the base airfoil are compared. As stated in the previous chapter the mesh used remained the same across simulations as well as the numerical setup which was already described in section 3.

Flow velocities studied included 50m/s, 90 m/s and 130m/s. This range encompasses a range suitable to take the pretended conclusions without entering in compressible flow regime in the upper range of injection velocity and without causing much flow perturbations due to velocity differences in the lower range. As for the angle of attack, when possible, five angle of attack were simulated ranging from 0 to 20 degrees. One of the main features of the coflow airfoil is that is said to improve stall behaviour, hence it was necessary to simulate airflow in angles of attack past stall conditions.

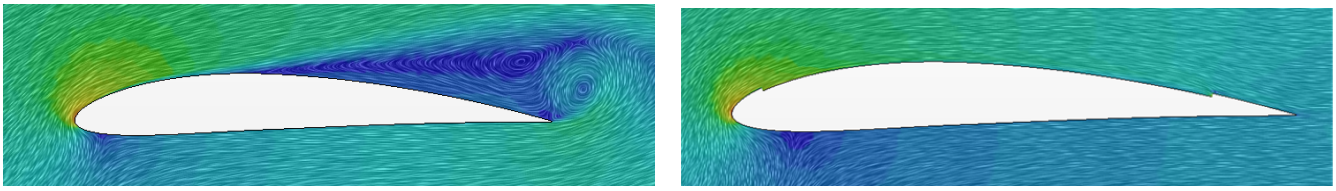

(a) Baseline (b) Coflow $U_{jet} = 130m/s$

Figure 3: Velocity field of simulations with $AoA = 20^{\circ}$

Main results are presented in Figs 4, with the baseline airfoil black colored. From these, it can be seen that three flow velocities increased the lift coefficient for all angles of attack, except for the 50m/s jet, which was not enough to avoid separation, with jet velocity lower than local flow velocity at the inlet position of the airfoil, which caused perturbations as will be explained later in this section. Furthermore, drag coefficient was higher for all jet velocities. This is due to the higher shear forces in the upper surface due to the higher velocity.

For the airfoil with jet velocity of 50m/s, instabilities were generated with the interactions between the higher moving flow and the jet flow, which deteriorate flow quality and causing separation. Flow velocity was not enough to overcome geometric differences caused by the gap. This way, convergence was not possible for higher angles of attack where this effects were more pronounced.

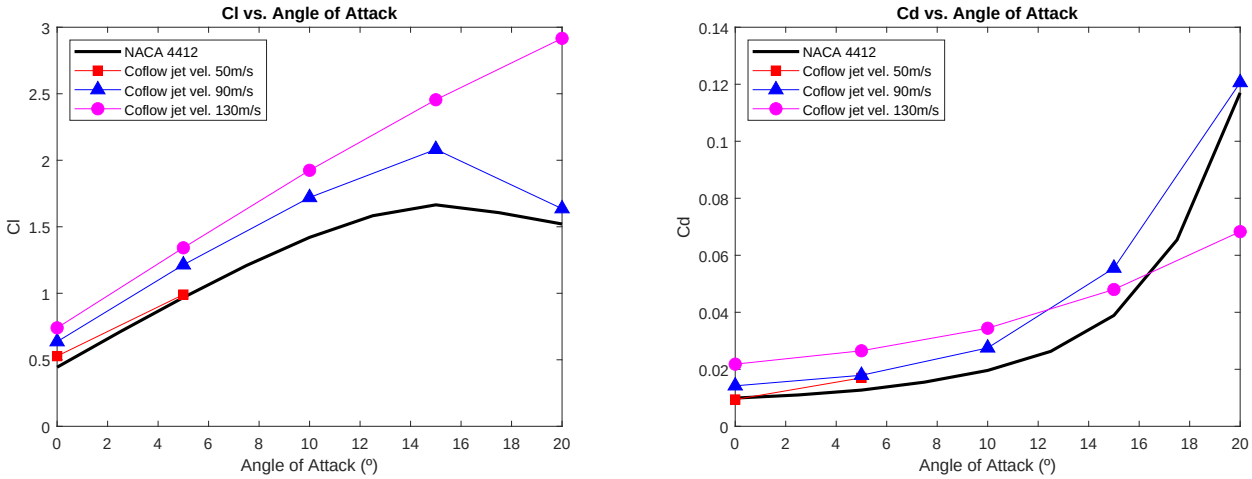

Figure 4: Simulation results for lift and drag coefficient versus angle of attack

Lift coefficient plot shows a clear advantage of using the coflow technology, with a linear behaviour far beyond the stall angle of the original airfoil. This is because separation does not occur for these jet velocities. As can be seen in Fig. 3, the flow remains attached, which also prevents the sudden increase in drag present on common airfoils when separation occurs.

This effect is better seen in the Cl/Cd analysis, which functions as an efficiency parameter allowing to analyse the combine effect in Cl e Cd. These results are shown in Fig. 5. This high lift behaviour is beneficial for aircrafts that require high maneuverability, which is usually associated with high lift maneuvers with applicability, for instance, in military fighters.

As previously mentioned, drag is higher when compared with the original NACA 4412 due to higher shear forces on the upper surface of the airfoil. This increase is caused by the higher velocities in that region. In addition, sudden increase in drag due to separation is also present, being aggravated by the instabilities of the detached jet. These results point to the necessity for accurate control of jet flow velocity.

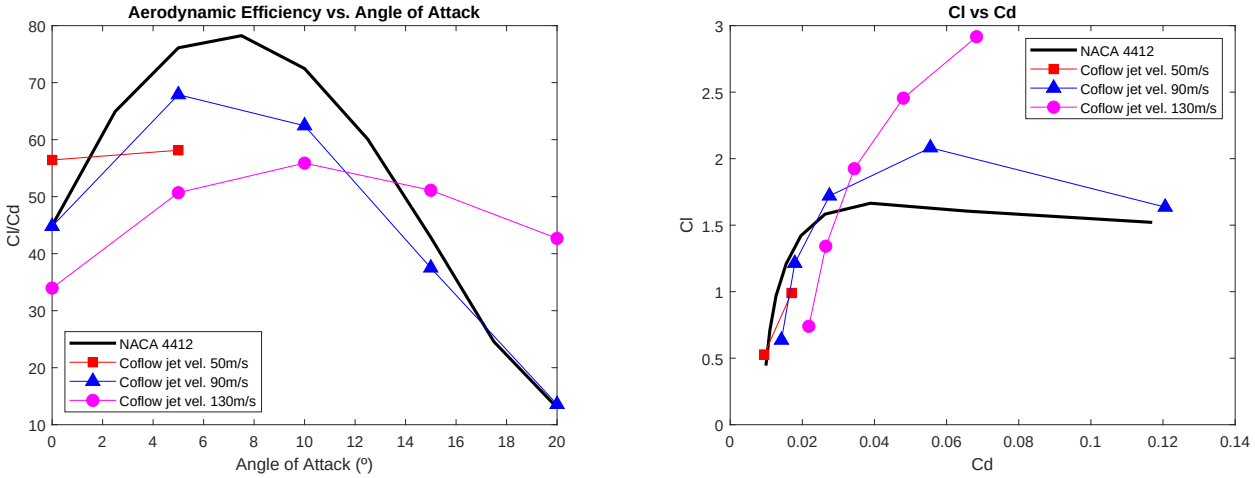

Figure 5: Simulation results for aerodynamic efficiency C_l/C_d versus angle of attack, and lift versus drag coeficients

From the analysis of the efficiency plots it can be concluded that despite the general increase in lift, the drag cost makes some jet velocities more suitable for specific angles of attack. Low velocity jets are more aerodynamic efficient for lower angles of attack whereas higher velocity jets seem to be the most appropriate for higher angles of attack. This way, methods of implementing this kind of boundary layer control may benefit from smaller geometric alterations to the original one, allowing complete turn off of the injected flow for some angles of attack, with minimal flow perturbations.

To note that the energy required to inject air, henceforth translated as the total pressure of the injected flow, is highly dependant on angle of attack and external flow velocity wanted. Assuming incompressible flow, total pressure is given by Bernoulli equation:

$$p_T = p + \frac{1}{2}\rho V^2 \tag{6}$$

It can be deduced the following relation for the total pressure required for the injection, where the index 1 indicates the position directly above the jet exit, which is directly dependant of angle of attack.

$$p_{T_{jet}} = \frac{1}{2}\rho(V_\infty^2 - V_1^2 + V_{jet}^2) \tag{7}$$

By the analysis of the equation, one can conclude that higher jet velocities and higher flying speeds require more energy for the injection. Changes in angle of attack will alter the velocity and thus pressure at jet exit which also influences energy required. Authors suggest this energy to be leaked directly from the engine. These are all considerations required to take into consideration when designing the implementation of this technology.

6 Conclusion

Many of the improvements stated by the coflow airfoil literature in comparison with the baseline airfoil were also observed in the results of this project. Lift coefficient increases significantly and stall conditions are delayed for appropriate jet velocities

in relation to the angle of attack and flow velocity. Despite that, the consensual drag coefficient improvements related by the literature were not observed in this study, with exception of the conditions after which the baseline airfoil had already stalled, where the delayed stall point of the coflow airfoil with the $130m/s$ jet clearly shows benefits.

This disparities observed in drag coefficient results could be a consequence of the mesh's high skewness close to the jet's inlet and outlet. It wasn't possible to correct this issue with the limited time available to complete this project. Nevertheless, this highly skewed volumes were present at the same location in each of the refinement levels, thus making the convergence study valid: if there was an error due to the skewness in this critical locations, this error was also present at a similar scale in the more refined meshes. The Richardson extrapolation method was used for the grid convergence study and was successful for both the baseline NACA 4412 and the coflow airfoils. The data validation of the baseline profile confirms that the computational model is accurate until the stalling point. There was no experimental data of the coflow airfoil to compare the obtained computation results.

As expected the computational results show that coflow airfoils delay flow separation. By reenergizing the boundary layer, the kinetic energy of the jet maintains the flow attached at higher angles of attack, which results in a better aerodynamic efficiency. The velocity of the jet should be catered to the angle of attack and external flow velocity, because if the jet velocity is lower than the velocity of the flow just above the jet inlet, there will be massive separation of the flow (as it was discussed for the coflow $U_{jet} = 50m/s$ case). A control system to obtain the optimal jet velocity for any flight conditions might prove to be very beneficial to this technology.

To improve this work, it is fundamental to improve the mesh at the jet's inlet/outlet to reduce skewness. After that, the convergence study should be done for each of the flow conditions, i.e, for each angle of attack and each jet velocity. Also, more jet velocities should have been tried in order to get a better understanding of what is the optimal one for each angle of attack.

7 Appendix

7.1 Mesh Details

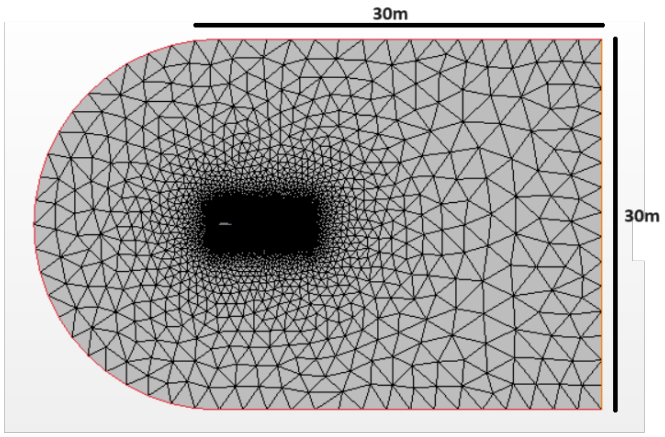

Figure 6: Computational Domain

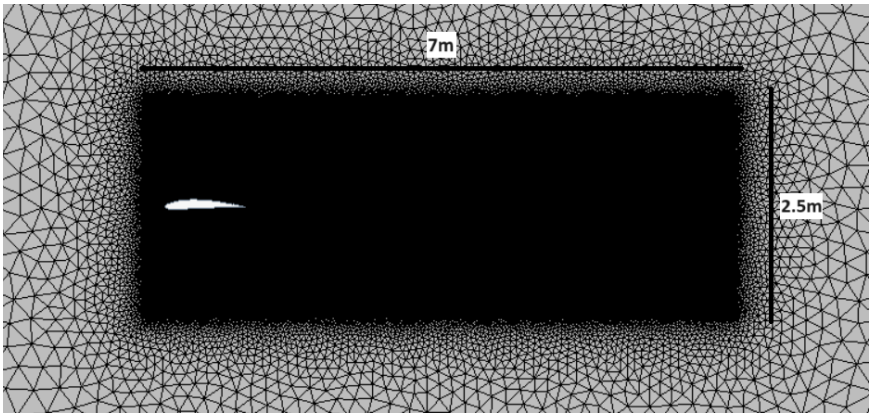

Figure 7: Detail Refinement Box

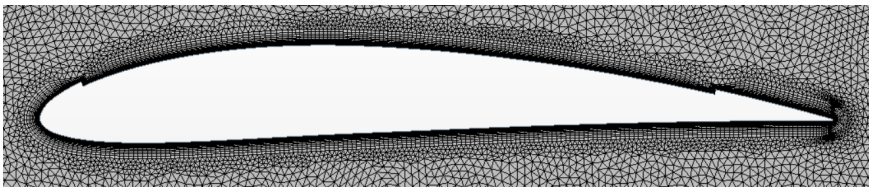

Figure 8: Detail Airfoil

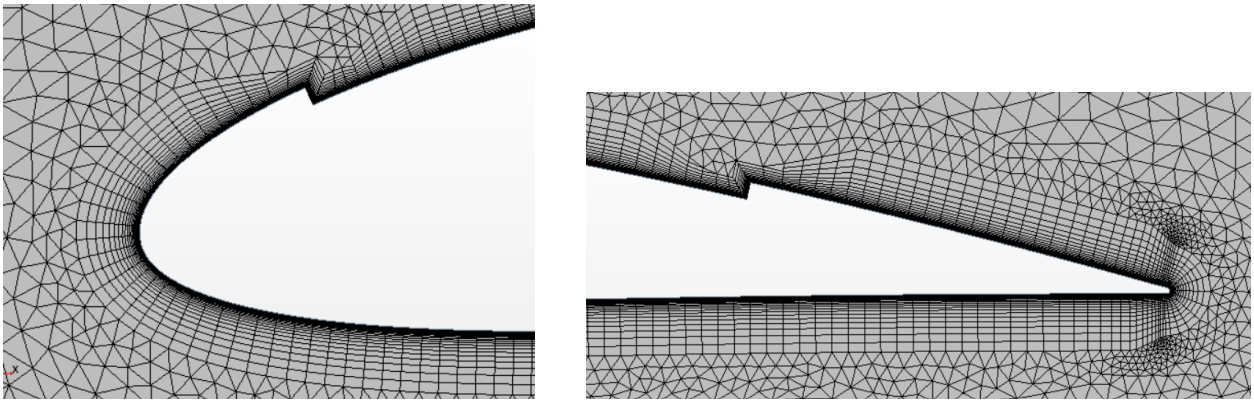

Figure 9: Leading and trailing edge details

Bibliography

[1] T. L. Chng, A. Rachman, H. M. Tsai, and G.-C. Zha, "Flow Control of an Airfoil via Injection and Suction," en, *Journal of Aircraft*, vol. 46, no. 1, pp. 291–300, Jan. 2009, ISSN: 0021-8669, 1533-3868. DOI: 10.2514/1.38394. [Online]. Available: https://arc.aiaa.org/doi/10.2514/1.38394 (visited on 12/11/2023).

[2] G.-C. Zha, W. Gao, and C. D. Paxton, "Jet Effects on Coflow Jet Airfoil Performance," en, *AIAA Journal*, vol. 45, no. 6, pp. 1222–1231, Jun. 2007, ISSN: 0001-1452, 1533-385X. DOI: 10.2514/1.23995. [Online]. Available: https://arc.aiaa.org/doi/10.2514/1.23995 (visited on 12/11/2023).

[3] G. Zha. "3d virtual simulation system of coflow jet airfoil with embedded micro-compressor actuator." PowerPoint Presentation. (2023), [Online]. Available: https://nas.nasa.gov/assets/nas/pdf/ams/2023/AMS_20230824_Zha.pdf.

[4] G.-C. Zha and C. Paxton, "A Novel Airfoil Circulation Augment Flow Control Method Using Co-Flow Jet," en, in *2nd AIAA Flow Control Conference*, Portland, Oregon: American Institute of Aeronautics and Astronautics, Jun. 2004, ISBN: 978-1-62410-030-7. DOI: 10.2514/6.2004-2208. [Online]. Available: https://arc.aiaa.org/doi/10.2514/6.2004-2208 (visited on 12/11/2023).

[5] G.-C. Zha, B. F. Carroll, C. D. Paxton, C. A. Conley, and A. Wells, "High Performance Airfoil Using Co-Flow Jet Flow Control," en,

[6] A. Lefebvre and G. Zha, "Numerical Simulation of Pitching Airfoil Performance Enhancement Using Co-Flow Jet Flow Control," en, in *31st AIAA Applied Aerodynamics Conference*, San Diego, CA: American Institute of Aeronautics and Astronautics, Jun. 2013. DOI: 10.2514/6.2013-2517. [Online]. Available: https://arc.aiaa.org/doi/10.2514/6.2013-2517 (visited on 12/11/2023).

[7] I. H. Abbott, A. E. Von Doenhoff, and L. Stivers Jr, "Summary of airfoil data," Tech. Rep., 1945.